pubs.acs.org/Biomac

Article

Pulmonary Pharmacokinetics of Polymer Lung Surfactants Following Pharyngeal Administration in Mice

Seyoung Kim, Daniel J. Fesenmeier, Sungwan Park, Sandra E. Torregrosa-Allen, Bennett D. Elzey, and You-Yeon Won*

Cite This: *Biomacromolecules* 2022, 23, 2471−2484

Read Online

ACCESS | Metrics & More | Article Recommendations | Supporting Information

ABSTRACT: We have recently discovered that pulmonary administration of nanoparticles (micelles) formed by amphiphilic poly(styrene−*block*−ethylene glycol) (PS−PEG) block copolymers has the potential to treat a lung disorder involving lung surfactant (LS) dysfunction (called acute respiratory distress syndrome (ARDS)), as PS−PEG nanoparticles are capable of reducing the surface tension of alveolar fluid, while they are resistant to deactivation caused by plasma proteins/inflammation products unlike natural LS. Herein, we report studies of the clearance pathways and kinetics of PS−PEG nanoparticles from the lung, which are essential for designing further preclinical IND-enabling studies. Using fluorescently labeled PS−PEG nanoparticles, we found that, following pharyngeal aspiration in mice, the retention of these nanoparticles in the lungs extends over 2 weeks, while their transport into other (secondary) organs is relatively insignificant. An analysis based on a multicompartmental pharmacokinetic model suggests a biphasic mechanism involving a fast mucociliary escalator process through the conducting airways and much slower alveolar clearance processes by the action of macrophages and also via direct translocation into the circulation. An excessive dose of PS−PEG nanoparticles led to prolonged retention in the lungs due to saturation of the alveolar clearance capacity.

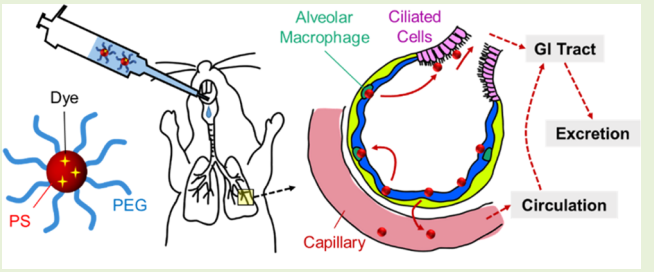

INTRODUCTION

Acute respiratory distress syndrome (ARDS) is a life-threatening respiratory condition characterized by severe hypoxemia and reduced respiratory compliance.[1] ARDS has a high prevalence (190,000 patients per year in the US)[2] and a high mortality rate (up to 45% depending on the severity of hypoxemia).[1] Moreover, the recent SARS-CoV-2 (COVID-19) pandemic has greatly increased the number of ARDS cases, as more than 15% of severely ill COVID-19 patients were reported to develop ARDS.[3,4] In ARDS lungs, acute lung injury (ALI) from aspiration of toxic substances (e.g., acids), pneumonia, sepsis, and other risk factors causes dysfunction of the lung surfactant (LS) monolayer that coats the surface of alveolar lining fluid.[5] Clinical trials have been performed to test whether supplying exogenous LS (extracted from animals) to a patient's lungs is able to reinforce alveolar lipid monolayer mechanics. Unfortunately, to date, this surfactant replacement therapy (SRT) has not been successful in treating ARDS,[6] including ARDS caused by COVID-19.[7] This lack of success is attributed to the deactivation of LS in inflamed lungs, caused by (i) enzymatic lysis of phospholipids during inflammation and/or (ii) contamination of the LS monolayer with plasma proteins released from capillary blood vessels surrounding the lungs.[5]

Our laboratory has been exploring a radically different approach, in which, instead of lipids, synthetic polymers are used as the active therapeutic ingredient (i.e., as the surface tension-reducing agent) in the SRT treatment of ARDS. Polymers are advantageous because they maintain their ability to control the dynamic surface tension of alveolar fluid even in the presence of LS bioinhibitors (i.e., inflammatory phospholipases and serum proteins). Specifically, we have demonstrated the therapeutic efficacy of a polymer lung surfactant (PLS) formulation in a mouse model of ALI (induced by acid aspiration).[8] PLS is composed of nanoparticles (micelles) formed by amphiphilic poly(styrene−*block*−ethylene glycol) (PS−PEG) block copolymers. PS−PEG micelles reduce the surface tension of water down close to zero under high compression, while this effect is unaffected by the presence of surface-active plasma proteins (such as albumin). Toxicological evaluation in mice showed that intrapharyngeally instilled PLS does not cause any symptoms of toxicity in terms of lung histology and the levels of inflammatory markers relative to control (treated with vehicle only) at 7 days after administration.[8] To support future IND-enabling studies in

Received: February 18, 2022
Revised: May 2, 2022
Published: May 17, 2022

https://doi.org/10.1021/acs.biomac.2c00221
Biomacromolecules 2022, 23, 2471−2484

large animals, a detailed investigation of the pharmacokinetics (PK) of PLS in mice is desirable.

Herein, we report an initial study of the kinetics and mechanisms of clearance of PLS from the lungs after pharyngeal aspiration in normal mice. From the PK standpoint, PLS (PS−PEG micelles) has two distinct characteristics; PS−PEG micelles are (i) biopersistent (i.e., nonresorbable) and (ii) charge neutral. A few reports have been documented on the pulmonary PK of biopersistent, PEG-coated (PEGylated) nanoparticles,[9−11] including PS−PEG nanoparticles,[12] which are chemically similar to but significantly larger (60−1000 nm in diameter) than our PLS nanoparticles (having ∼30 nm diameter). Currently, there is no data available in the literature about the long-term fate of biopersistent PEGylated nanoparticles at time scales >1 month following pulmonary administration.

In this work, the lung retention/clearance, organ biodistribution, and total body clearance characteristics of PLS instilled into the lungs of mice were evaluated over a period of 56 days. PLS nanoparticles were labeled with a hydrophobic fluorescent dye (DiR) for the quantitative determination of PLS content in organs, blood, urine, and feces as a function of time. The primary focus of the study was to characterize the retention of PLS in the alveolar space where its pharmacological effect (i.e., regulation of the alveolar surface tension by PLS) takes place. Experimental data were fit to a multicompartmental pulmonary PK model that takes into account all major mechanisms of nanoparticle clearance from the lungs (mucociliary escalator, phagocytosis by macrophages, and translocation into the circulation through the blood−air barrier).[12,13] The PK properties of PLS were studied at two different PLS dose concentrations to probe the effect of PLS concentration since dose concentration is an important parameter that influences the efficacy and safety of pulmonary nanoparticle use.[14] Potential issues associated with excess PLS doses (possible inflammation and metabolic dysfunction in the lung) are also briefly discussed; further study is ongoing.

EXPERIMENTAL PROCEDURES

Materials and Reagents. Poly(ethylene glycol) monomethyl ether (PEG−OH, M_n = 5,000 g/mol), 4-cyano-4-[(dodecylsulfanylthiocarbonyl)sulfanyl] pentanoic acid (CDTPA), 4-dimethylaminopyridine (DMAP), *N*,*N*′-dicyclohexylcarbodiimide (DCC), 2,2′-azobis(isobutyronitrile) (AIBN), dichloromethane (DCM), deuterated dichloromethane-d_2 (DCM-d_2), 1,4-dioxane, Triton X-100, and sodium chloride (NaCl) were purchased from Sigma-Aldrich and used as received. *n*-Hexane, diethyl ether, acetone, *N*,*N*-dimethyl formamide (DMF), and ethyl acetate (EA) were purchased from Fisher Scientific and used as received. Anhydrous styrene (Sigma-Aldrich) was purified with activated alumina (Sigma-Aldrich) before use. 1,1′-Dioctadecyl-3,3,3′,3′-tetramethylindotricarbocyanine iodide (DiR) was purchased from Invitrogen.

Synthesis and Characterization of PS−PEG. The PS−PEG polymer used was synthesized by Reversible Addition−Fragmentation Chain Transfer (RAFT) polymerization using the previously reported procedure.[8] Briefly, a RAFT agent, CDTPA, was conjugated to PEG−OH by Steglich esterification in the presence of DMAP and DCC in DCM. The product, PEG−CDTPA, was triply purified by precipitation in a 1:1 (by volume) mixture of hexane and diethyl ether. After drying under vacuum, the purified PEG−CDTPA was co-dissolved with AIBN in 1,4-dioxane, and the solution was degassed with three freeze−pump−thaw cycles. Then, styrene was introduced into the mixture to initiate the RAFT polymerization. The polymerization reaction was run for 20 h at 75 °C and terminated by exposing the reaction mixture to air. The resulting PS−PEG product was triply precipitated in a 1:1 (by volume) mixture of hexane and diethyl ether and then dried under vacuum.

The synthesized PS−PEG polymer was characterized by ^{1}H NMR spectroscopy using a Bruker ARX NMR spectrometer operating at 500 MHz. For this measurement, the polymer was dissolved in DCM-d_2 at a concentration of 3 wt %. From the ratio of the peak areas for the phenyl protons of PS (δ = 7.5−6.0 ppm) to the peak areas for the ether protons of PEG (δ = 3.9−3.0 ppm), the number-average molecular weight of the PS block was estimated to be $M_{n,PS}$ = 5,887 g/mol. The overall molecular weight polydispersity index (PDI) was characterized by gel permeation chromatography (GPC) using an Agilent Technologies 12000 Series instrument equipped with a Hewlett-Packard G1362A refractive index (RI) detector and three PLgel 5 μm MIXED-C columns. THF was used as the mobile phase at a flow rate of 1 mL/min at 35 °C. Based on calibration with PS standards (Agilent Easi Cal), the PDI of the PS−PEG was estimated to be M_w/M_n = 1.14.

Preparation and Characterization of PS−PEG Nanoparticles (micelles). Pristine PS−PEG nanoparticles (micelles) and also PS−PEG nanoparticles loaded with a hydrophobic fluorescence dye, DiR, were prepared via the Flash NanoPrecipitation (FNP) technique under an identical condition.[15] PS−PEG was dissolved in acetone at a concentration of 12 mg/mL, and the solution was filtered through a poly(tetrafluoroethylene) (PTFE) syringe filter with a 0.45 μm pore size. Separately, DiR was dissolved in acetone (pre-filtered with a 0.45 μm PTFE filter, pre-filtered to avoid possible loss of DiR by adsorption to the filter material) at a concentration of 2 mg/mL. The PS−PEG and DiR solutions were mixed at a volume ratio of 5:1 to produce a feed solution containing PS−PEG and DiR at an initial mass ratio of 30:1. The feed solution (1.0 mL) was charged in a 1 mL Norm-Ject syringe (inner diameter = 4.7 mm), which was connected to an inlet port of a NanoFabTx microfluidic mixer (Sigma-Aldrich). The other inlet port of the microfluidic mixer was connected to a 10 mL Norm-Ject syringe (inner diameter = 15.9 mm) charged with 10 mL of Milli-Q-purified water. The two syringes were then simultaneously pumped using a dual-syringe infusion pump (KD Scientific) at an identical linear pumping speed (at a total flow rate of the liquids of 1.24 mL/min); rapid mixing was achieved at a volumetric ratio of 1:11.4 between the acetone solution and water. The resulting mixture was collected through an outlet port, and the residual acetone content in the mixture was removed by 3 cycles of centrifugal dialysis against cold Milli-Q water using an Amicon Ultra-15 filter unit with a 10 kDa molecular weight cutoff (MWCO) membrane (Millipore). The concentrated solution was collected and adjusted with 5 wt % NaCl (aq.) to produce a final PS−PEG nanoparticle solution in 0.9 wt % NaCl. PS−PEG nanoparticles without loaded DiR ("pristine" PS−PEG nanoparticles) were prepared using the exact same FNP procedure as for DiR-loaded PS−PEG nanoparticles.

DiR-loaded and pristine PS−PEG nanoparticles were characterized by transmission electron microscopy (TEM) using a 200 kV Tecnai T20 instrument. PS−PEG nanoparticles prepared in Milli-Q water (instead of saline) were negatively stained with 2% uranyl acetate (to enhance the contrast between the nanoparticle and the background) and then dried on a carbon-coated grid. The hydrodynamic size of pristine PS−PEG nanoparticles was measured by dynamic light scattering (DLS) using a Brookhaven NanoBrook 90Plus instrument. For this measurement, the nanoparticle solution was diluted to 0.5 mg/mL in 0.9 wt % NaCl and filtered using a nylon mesh filter (pores of 0.22 μm). The DLS measurement was performed at a scattering angle of 90° and a laser wavelength of 640 nm. DiR-loaded PS−PEG nanoparticles could not be characterized by DLS because DiR absorbs at 640 nm.

Fluorescence spectra for DiR-loaded PS−PEG nanoparticles were recorded using a BioTek Synergy Neo microplate reader at an excitation wavelength of 745 nm. A 0.6 mg/mL solution of DiR-loaded PS−PEG nanoparticles in Milli-Q water was diluted with a 2:1 by volume mixture of DMF and Triton X-100 to a desired nanoparticle concentration. The final nanoparticle solution (180 μL) was loaded into a 96-well black polypropylene plate. The stability

https://doi.org/10.1021/acs.biomac.2c00221
Biomacromolecules 2022, 23, 2471−2484

of DiR-loaded PS−PEG nanoparticles (i.e., the lack of uncontrolled release of DiR) was tested for 4 weeks in vitro; a solution containing 0.2 mg/mL DiR-loaded PS−PEG nanoparticles in phosphate-buffered saline (PBS) was incubated at 37 °C, and a small amount of the solution was sampled at regular intervals during the 4-week period for fluorescence analysis at 745 nm excitation and 790 nm emission.

Pharmacokinetics (PK) and Biodistribution (BD) of PS−PEG Nanoparticles. The mouse study protocol was approved by Purdue Institutional Animal Care and Use Committee (PACUC) (Approval No. 1112000342) and conforms to the NIH animal care guidelines. The pharmacokinetics of PS−PEG nanoparticles was evaluated following intrapharyngeal administration in C57BL/6 mice (8−12 weeks old, female, ∼20 g body weight) in three different groups: (i) mice dosed with 80 μL of a 0.6 mg/mL solution of DiR-loaded PS−PEG nanoparticles in normal saline (NS, 0.9% NaCl) (group 1), (ii) mice dosed with 80 μL of a 6.0 mg/mL solution of DiR-loaded PS−PEG nanoparticles in NS (group 2), and (iii) mice dosed with 80 μL of a 6.0 mg/mL solution of pristine PS−PEG nanoparticles in NS (group 3, control). Prior to pharyngeal instillation, each mouse was anesthetized with isoflurane and then laid on the back on a 75° tilted surface with its incisors hung on a wire. The tongue was pulled out of the mouth using forceps, and 80 μL of PS−PEG nanoparticle suspension was directly dropped into the pharynx using a micropipette (called the tongue-pull technique), while the opening of the pharynx into the larynx was monitored using an illuminated otoscope (RW-A3749, Welch Allyn).[16] After the instillation procedure, the mouse was left to naturally recover from anesthesia.

Mice in groups 1 and 2 were humanely sacrificed at 1, 3, 7, 14, 21, 28, 42, and 56 days after PS−PEG instillation (N = 4 per group per time point). Four mice in group 3 were sacrificed 1 day after PLS instillation. Organ and blood specimens were collected from euthanized mice, and their wet masses were recorded. Fluorescence images of excised organs were acquired using an AMI imager (Spectral Instruments, USA) at excitation and emission wavelength settings of 745 and 790 nm, respectively. At different times, body weights were monitored, and excreted feces were collected for a 1 day sampling period at each time point from the subgroups of mice (N = 4) in groups 1 and 2 that were sacrificed at 56 days. Excreted urine was also collected on filter paper placed in the cages at different times. The amounts of PS−PEG nanoparticles retained in the lungs, translocated into secondary organs, and excreted as feces through the gastrointestinal tract (GIT) were quantitated using the procedures described below. Experimental PK/BD data were fit to a multicompartmental PK model described in the Theoretical Model & Analysis Procedures section.

Quantitation of PS−PEG Nanoparticle Concentrations in Mouse Tissues by Fluorescence Measurements. Organs, blood, and feces collected at different time points were analyzed for DiR contents. 0.2 mL of 25% Triton X-100 solution in Milli-Q water was added to a weighted tissue sample, and the mixture was homogenized using a bead mill homogenizer at 5500 rpm. When necessary, the sample was divided (i.e., cut using dissecting scissors) into multiple portions so that the amount of the tissue analyzed did not exceed 500 mg per homogenization tube. The resulting tissue homogenate was taken and extracted with a mixture of 0.2 mL of ethyl acetate and 0.1 mL of 25% Triton X-100 in water three times. In each extraction run, the mixture was homogenized and centrifuged. The supernatant was collected and dried under vacuum for 24 h, which left a pellet containing DiR with about 0.1 mL of nonvolatile Triton X-100. The pellet was redispersed in 0.2 mL of DMF by vortexing; the final solvent composition was DMF/Triton X-100 (∼2:1 by volume). The fluorescence intensities of these solutions were measured using a BioTek Synergy Neo microplate reader at excitation and emission wavelengths of 745 and 790 nm, respectively. Fluorescence intensities were translated to DiR-loaded PS−PEG nanoparticle concentrations using an intensity vs. concentration calibration obtained with extracts prepared from DiR-loaded nanoparticle suspensions with known nanoparticle concentrations (prepared in Milli-Q water) using the exact same liquid−liquid extraction procedure as for the tissue homogenate samples; the calibration study is discussed in the Results section.

Micro-CT Imaging of Instilled PS−PEG Nanoparticle-Containing Contrast Media. Instantaneous distribution of pharyngeally instilled PS−PEG nanoparticle-containing contrast media was evaluated in situ using a Quantum GX Micro-CT imaging system (PerkinElmer). C57BL/6 mice (8−12 weeks old, female, ∼20 g body weight) were dosed with 80 μL of an aqueous contrast medium containing pristine PS−PEG nanoparticles (0.6 mg/mL) and a water-soluble X-ray contrast agent, Iohexol (50 mg iodine/mL) in NS. Pharyngeal administration was done using the same procedure as for the PK/BD study. Immediately after pharyngeal administration of the contrast medium, the animal was subject to micro-CT imaging without disturbing anesthesia. The scan time was 4 min at a voltage of 90 kV, a current of 88 μA, and a field of view (FOV) of 45 mm. Contrast medium distribution was quantitated using the procedure described below.

Quantitative Analysis of Micro-CT Images. Micro-CT images were analyzed using ImageJ software. Areas of interest were identified and manually segmented out from image stacks. A binary mask was applied to the areas of interest such that only the regions containing the contrast agent retained nonzero intensity values. The "and" image operator was then applied to the segmented binary masked image and the original segmented image such that the intensity values for the regions containing the contrast agent were returned to their original value and all other regions were set to 0. The three-dimensional (3D) object counter algorithm was then applied to calculate the integrated density of each region, which was used as the proxy for the total amount of the contrast agent present in each region.

THEORETICAL MODEL & ANALYSIS PROCEDURES

A multicompartmental PK model was developed in which the lung system is divided into two compartments—the bronchia and alveoli (Figure 7 of the Results section). The PS−PEG nanoparticle instillation process is described as an instantaneous supply of bolus of a nanoparticle solution into three separate compartments, i.e., alveoli (A), conducting airways (B), and larynx (L), with respective nanoparticle number fractions of $f_{A,0}$, $f_{B,0}$, and $f_{L,0}$ ($f_{A,0} + f_{B,0} + f_{L,0} = 1$). The fraction of PS−PEG nanoparticles initially deposited in the larynx was fixed at $f_{L,0} = 0.27$ on the basis of a micro-CT scan (Figure 6). The first-order kinetics was assumed for all nanoparticle transport processes in and out of individual compartments, including (i) transport of nanoparticles by alveolar macrophages from the alveolar space to conducting airways (which is characterized by a rate constant k_A), (ii) clearance of nanoparticles by mucociliary action from conducting airways toward the larynx and eventually toward the gastrointestinal tract (GIT) (characterized by a rate constant k_B), (iii) diffusive translocation ("transepithelial diffusion") of nanoparticles through the blood−air barrier (BAB) into the systemic circulation or through the epithelial barrier into the lymph and then eventually into the circulation (characterized by a combined rate constant k_T), and (iv) ultimate clearance of the nanoparticles from the body (mainly) via the hepatobiliary system (i.e., via the liver) (characterized by a rate constant k_C). The assumption of first-order kinetics is supported by previous research on the kinetics of macrophage-mediated clearance,[14,17] mucociliary transport,[18,19] transepithelial diffusion,[20] and systemic circulation.[21]

Based on the mechanistic scheme shown in Figure 7, kinetic nanoparticle mass balance equations for individual tissue compartments can be written as follows

$$\frac{dN_A(t)}{dt} = -(k_A + k_T)N_A(t) \quad (1a)$$

https://doi.org/10.1021/acs.biomac.2c00221
Biomacromolecules 2022, 23, 2471−2484

$$\frac{dN_B(t)}{dt} = k_A N_A(t) - k_B N_B(t) \quad (1b)$$

$$\frac{dN_C(t)}{dt} = k_T N_A(t) - k_C N_C(t) \quad (1c)$$

$$\frac{dN_E(t)}{dt} = k_B N_B(t) + k_C N_C(t) \quad (1d)$$

where $N_A(t)$, $N_B(t)$, $N_C(t)$, and $N_E(t)$ are, respectively, the time-dependent amounts (numbers or masses) of PS−PEG nanoparticles in the alveolar space, conducting airways, systemic circulation (including excretory organs), and fecal excretion. Further, it is assumed that PS−PEG nanoparticles cleared from the mucociliary escalator and from the liver are excreted via the GIT (eq 1d). The initial conditions used are $N_A(0) = N_{A,0} = f_{A,0}N_0$, $N_B(0) = N_{B,0} = f_{B,0}N_0$, $N_C(0) = 0$, and $N_E(0) = f_{L,0}N_0$, where N_0 is the amount (number or mass) of initially administered PS−PEG nanoparticles. The mass balance equations in eq 1 have the following analytic solutions

$$N_A(t) = N_{A,0}\, e^{-(k_A+k_T)t} \quad (2a)$$

$$N_B(t) = k_A^* N_{A,0}\, e^{-(k_A+k_T)t} + (N_{B,0} - k_A^* N_{A,0}) e^{-k_B t} \quad (2b)$$

$$N_C(t) = k_T^* N_{A,0}(e^{-(k_A+k_T)t} - e^{-k_C t}) \quad (2c)$$

where $k_A^* = k_A[k_B - (k_A + k_T)]^{-1}$ and $k_T^* = k_T[k_C - (k_A + k_T)]^{-1}$. For comparison with the experiment, the amounts of PS−PEG nanoparticles remaining in the lungs at time t ($N_{lung}(t)$) and excreted in the feces during a 24 h period at time t ($\Delta N_E(t)$) can be calculated as follows

$$N_{lung}(t) = N_A(t) + N_B(t) = (1 + k_A^*)N_{A,0}\, e^{-(k_A+k_T)t} + (N_{B,0} - k_A^* N_{A,0}) e^{-k_B t} \quad (3a)$$

$$\Delta N_E(t) = \int_{t-\Delta t}^{t} \frac{d}{d\tilde{t}} N_E(\tilde{t})\, d\tilde{t} = (1 + k_A^* + k_T^*)N_{A,0}(e^{(k_A+k_T)\Delta t} - 1)e^{-(k_A+k_T)t} + (N_{B,0} - k_A^* N_{A,0})(e^{k_B \Delta t} - 1)e^{-k_B t} - k_T^* N_{A,0}(e^{k_C \Delta t} - 1)e^{-k_C t} \quad (3b)$$

where Δt is the time duration of feces sample collection (=24 h).

This PK model has 5 unknowns: $N_{A,0}$, k_A, k_B, k_T, and k_C. Note that $N_{B,0}$ is given by $N_{B,0} = [1 - (f_{A,0} + f_{L,0})]N_0$. To reduce the number of fitting parameters, eq 3a was simplified to the following form

$$N_{lung}(t) = N_{slow}\, e^{-(k_A+k_T)t} + N_{fast}\, e^{-k_B t} \quad (4)$$

where the lung clearance process is a combination of a fast and a slow process; it is well known in the literature that the mucociliary clearance is far faster than the macrophage-mediated clearance or transepithelial diffusion ($k_B \gg k_A + k_T$).[12] Further, since $k_A^* \ll 1$

$$N_{slow} = (1 + k_A^*)N_{A,0} \cong N_{A,0} \quad (5a)$$

$$N_{fast} = N_{B,0} - k_A^* N_{A,0} \cong N_{B,0} \quad (5b)$$

Assuming that the hepatobiliary clearance is much faster than the macrophage-mediated clearance or the transepithelial diffusion (i.e., $k_C \gg k_A + k_T$ and thus $k_T^* \ll 1$),[22] eq 3b also reduces to a biexponential model

$$\Delta N_E(t) \cong N_{A,0}(e^{(k_A+k_T)\Delta t} - 1)e^{-(k_A+k_T)t} + N_{B,0}(e^{k_B \Delta t} - 1)\, e^{-k_B t} \quad (6)$$

Equations 4 and 6 were simultaneously fit to respective experimental data (shown in Figures 3 and 5, respectively) with four adjustable parameters, $N_{A,0}$, $N_{B,0}$, $(k_A + k_T)$, and k_B; the values of the other parameters (k_A, k_T, and k_C) could not be determined. The best-fit parameter values are summarized in Table 1. From the values of $N_{A,0}$ and $(k_A + k_T)$, the retention half-life ($t_{1/2,A}$) and total time-integrated amount (AUC_A) of PS−PEG nanoparticles within the alveolar space could be estimated (Table 1)

$$t_{1/2,A} = \frac{\ln(2)}{k_A + k_T} \quad (7a)$$

$$AUC_A = \int_0^\infty N_A(t)dt = \frac{N_{A,0}}{k_A + k_T} \quad (7b)$$

Similarly, the retention half-life ($t_{1/2,B}$) of PS−PEG nanoparticles in the conducting airways could also be estimated (Table 1)

$$t_{1/2,B} = \frac{\ln(2)}{k_B} \quad (8)$$

Table 1. Results of the Fitting Analysis of the Data Shown in Figures 2B, 3, and 5 Using the Multicompartmental PK Model Discussed in the Theoretical Model & Analysis Procedures Section

parameter (units)	value for group 1 (0.6 mg/mL)	value for group 2 (6.0 mg/mL)
$f_{A,0}$ [a]	0.019 ± 0.007	0.011 ± 0.003
$f_{B,0}$ [a]	0.71 ± 0.01	0.72 ± 0.00
$f_{L,0}$ [a,b]	0.27	0.27
$k_A + k_T$ (1/day) [a]	0.043 ± 0.010	0.024 ± 0.016
k_B (1/day) [a]	1.9 ± 0.7	2.2 ± 0.2
$t_{1/2,A}$ (days) [a]	16 ± 4	29 ± 20
$t_{1/2,B}$ (days) [a]	0.36 ± 0.13	0.32 ± 0.03
AUC_A (μg·days) [a]	21 ± 9	220 ± 160
$I_{A,0}$ ($\times 10^{10}$ photons/s) [c]	2.1 ± 0.1	7.2 ± 1.0
$I_{B,0}$ ($\times 10^{10}$ photons/s) [c]	7.8 ± 1.7	0 ± 72
$N_{A,0}$ (μg) [d]	2.5 ± 0.2	8.5 ± 1.2
$N_{B,0}$ (μg) [d]	9.3 ± 2.0	0 ± 85
$f_{A,0}$ [d]	0.053 ± 0.003	0.018 ± 0.003
$f_{B,0}$ [d]	0.19 ± 0.04	0.0 ± 0.2

[a] Best-fit PK parameter values for pharyngeally instilled DiR-loaded PS−PEG nanoparticles at two different dose concentration conditions (groups 1 and 2), obtained by fitting nanoparticle lung retention/feces excretion data in Figures 3 and 5 simultaneously to the multicompartmental PK model (eqs 4 and 6, respectively). [b] The value of $f_{L,0}$ was fixed at 0.27 based on the CT result (Figure 6). [c] Results obtained by fitting lung fluorescence data are shown in Figure 2B to eq 9. See relevant sections of the main text and also the figure caption for Figure 2B for details. [d] Values of $N_{A,0}$ and $N_{B,0}$ estimated from the values of $I_{A,0}$ and $I_{B,0}$, respectively, using the correlation shown in Figure S8. $f_{A,0} = N_{A,0}/N_0$ and $f_{B,0} = N_{B,0}/N_0$ where N_0 = 48 μg (group 1) and 480 μg (group 2).

https://doi.org/10.1021/acs.biomac.2c00221
Biomacromolecules 2022, 23, 2471−2484

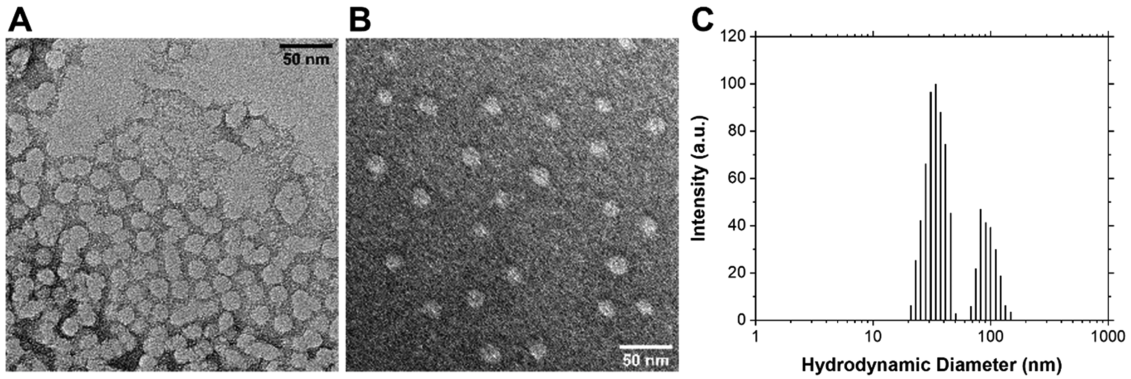

Figure 1. Representative TEM images of (A) DiR-loaded and (B) pristine PS−PEG nanoparticles. Specimens were negatively stained with uranyl acetate and dried. (C) DLS intensity vs. size histogram for pristine PS−PEG nanoparticles in 0.9% saline.

Equation 4 suggests that the fluorescence intensity estimated from whole lung images (Figure 2B) must also exhibit a similar biexponential decay, which can be described by

$$I(t) = I_{A,0}\, e^{-(k_A+k_T)t} + I_{B,0}\, e^{-k_B t} \quad (9)$$

Data in Figure 2B were fit to eq 9 above using $I_{A,0}$ and $I_{B,0}$ as adjustable parameters (best-fit values given in Table 1) while keeping the other parameters ($(k_A + k_T)$ and k_B) fixed, as previously determined (Table 1).

RESULTS

Preparation and Characterization of Fluorescently Labeled PS−PEG Nanoparticles. Nanoparticles (micelles) formed by poly(styrene−*block*−ethylene glycol) (PS−PEG) block copolymers were investigated as they are candidate polymer lung surfactant (PLS) therapeutic agents. For this study, a PS−PEG material with a narrow-molecular-weight distribution was synthesized by reversible addition−fragmentation chain transfer (RAFT) polymerization using a premade monomethoxy-monohydroxy-terminated PEG (mPEG-OH) as a precursor. The number-average molecular weight (M_n) of the PS block was determined by ^{1}H NMR to be M_n = 5.9 kg/mol. The molecular weight of the mPEG-OH precursor was M_n = 5.0 kg/mol. The polydispersity index (PDI) of the PS−PEG product was determined by GPC to be PDI = 1.14 (Figures S1 and S2). Due to an interplay of the strong hydrophobicity of PS and the amphiphilicity of PEG, PS−PEG nanoparticles have dualistic characteristics: (i) a strong affinity for the air−water interface and (ii) colloidal stability in the bulk water phase. This unique quality of PS−PEG micelles enables them to produce extremely low surface tension (high surface pressure) via formation of an insoluble close-packed micelle monolayer at the air−water interface.[8,23]

For ex vivo imaging and quantitation of PS−PEG micelle concentrations in major organs, blood, feces, etc., a hydrophobic near-IR dye, 1,1′-dioctadecyl-3,3,3′,3′-tetramethylindotricarbocyanine iodide (DiR, excitation and emission maxima at 745 and 790 nm, respectively), was physically loaded into the PS core domains of PS−PEG micelles using the Flash NanoPrecipitation (FNP) method;[15,24] as water is added to an acetone solution containing PS−PEG and DiR (log $P_{DiR/water}$ = 8.74), the solvent quality is reduced for both PS and DiR, and DiR becomes encapsulated within the hydrophobic core domain formed by the PS segments. DiR is kinetically trapped inside the core domain because of the glassy nature of the PS matrix at physiological temperature.[25,26] An FNP micromixer device enabled rapid mixing of the acetone solution with water at a volumetric ratio of 1:11.4 within 0.2 s, resulting in a complete exchange of the solvent from acetone to water. The loading content of DiR (defined as the mass of DiR encapsulated divided by the combined mass of PS−PEG and DiR in the micelle core) was optimized to a level of 3.2% (based on initial stoichiometry) to maximize the fluorescence intensity per nanoparticle; at higher DiR content, the fluorescence decreased because of the self-quenching effect.[27] Pristine PS−PEG nanoparticles (with no loaded DiR) were also prepared using the exact same FNP procedure.

After residual acetone was removed from the FNP product by repeated dialysis, PS−PEG nanoparticles were characterized by transmission electron microscopy (TEM) and dynamic light scattering (DLS). TEM data confirmed that DiR-loaded PS−PEG nanoparticles have identical shape and size characteristics to pristine PS−PEG nanoparticles; both nanoparticles were of spherical shape, and their dried diameters were D = 16.6 ± 1.5 nm (DiR-loaded) and 16.3 ± 1.2 nm (pristine) (Figure 1A,B). Thus, DiR loading is unlikely to alter the PK properties of PS−PEG nanoparticles. DLS gave information about the hydrodynamic diameter (D_H) of PS−PEG nanoparticles in NS, which includes the thickness of the hydrated PEG corona. The intensity-weighted DLS histogram of pristine PS−PEG nanoparticles showed a bimodal size distribution with a major population at D_H = 32 nm (representing 71% of the total intensity) and a minor population at D_H = 90 nm (larger aggregates) (Figure 1C). Cumulant analysis of the DLS data gave a z-average hydrodynamic diameter of $D_{H,z}$ = 39 nm and a polydispersity index of 0.18 for pristine PS−PEG nanoparticles. Note that considering that the scattering intensity scales with the particle size to the sixth power,[24] the large aggregates represent only a negligible fraction (~2% by volume) of the total population. Also of note, although the size characteristics of the present micelles (D = 16.3 ± 1.2 nm and D_H = 32 nm, prepared from PS(5.9k)−PEG(5.0k) by FNP) are somewhat different from those reported in our previous study (D = 20.0 ± 1.7 nm and D_H = 27 nm, micelles prepared from PS(5.6k)−PEG(5.0k) by a solvent exchange method),[8] the present PS−PEG nanoparticles were confirmed to exhibit high surface pressure (~70 mN/m) at high compression (Figure S3), which is a required attribute for a candidate PLS formulation.

The stability of DiR-loaded PS−PEG nanoparticles was evaluated at physiological conditions in vitro. A 0.2 mg/mL solution of DiR-labeled PS−PEG nanoparticles in PBS was

https://doi.org/10.1021/acs.biomac.2c00221
Biomacromolecules 2022, 23, 2471−2484

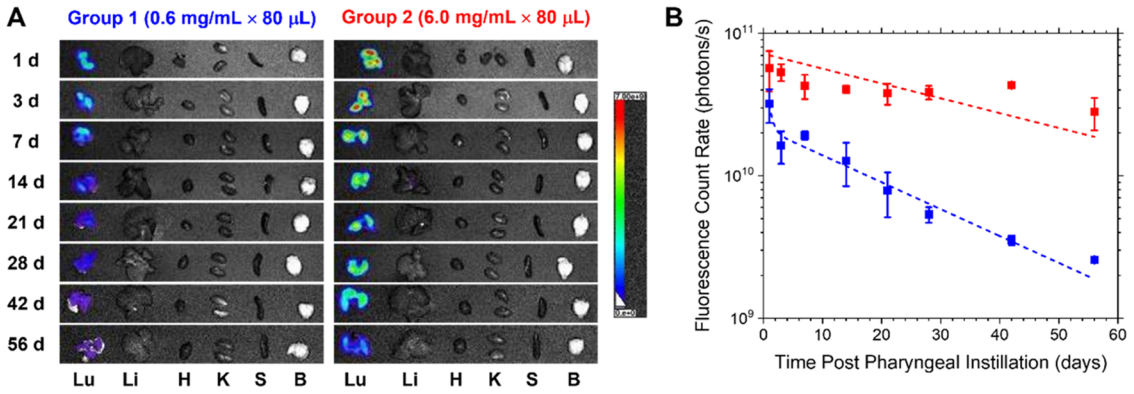

Figure 2. (A) Representative ex vivo overlaid fluorescence images of major organs collected at different times following pharyngeal instillation of DiR-loaded PS−PEG nanoparticles at two different dose concentrations. Lu = lungs; Li = liver; H = heart; K = kidneys; S = spleen; and B = brain. In the color scale bar, fluorescence radiance values are given in units of photons/s/cm^2/sr. (B) Average fluorescence count rate ($I(t)$) from the region of interest (ROI) of the lungs ex vivo as a function of time after pharyngeal instillation of DiR-loaded PS−PEG nanoparticles at the two different nanoparticle concentrations (N = 4, error bar = SD in a linear scale). Dashed lines represent fits to a double-exponential decay function ($I(t) = I_{A,0}\, e^{-(k_A+k_T)t} + I_{B,0}\, e^{-k_B t}$ (eq 9)) obtained using $I_{A,0}$ and $I_{B,0}$ as fitting parameters (best-fit values are given in Table 1); the alveolar and airway clearance rate constants ($(k_A + k_T)$ and k_B, respectively) were fixed at values obtained by fitting the data in Figures 3 and 5 simultaneously to the multicompartmental PK model (i.e., eqs 4 and 6, respectively) (values given in Table 1).

incubated at 37 °C for 4 weeks, and during that period, the fluorescence intensity was measured at regular intervals (Figure S4); at each time point, an aliquot (0.15 mL) was taken from the stock solution and used for analysis because the process of intensity measurement itself causes photobleaching. No significant changes in fluorescence intensity were observed, indicating that no chemical degradation or leaching of DiR from the nanoparticles had occurred after formation. This result is consistent with the fact that DiR is chemically stable at neutral pH,[28] and the glassy character of the PS core domain suppresses the diffusion of the DiR molecules. Because the intensity trend did not show any indication of a slope change, the measurement was not continued beyond 4 weeks.

A DiR fluorescence intensity vs. PS−PEG nanoparticle concentration calibration curve was constructed as follows: 0.45 mL of a 2:1 by volume mixture of DMF and Triton X-100 was added to 0.05 mL of a premade Milli-Q water solution containing a known concentration of DiR-loaded PS−PEG nanoparticles. Similar mixtures were prepared at different initial PS−PEG nanoparticle concentrations. Fluorescence spectra for these mixtures were measured. A fluorescence maximum at around 790 nm was verified (Figure S5A), and the intensity values measured at this wavelength were used to construct an intensity vs. concentration calibration curve (Figure S5B). A linear dependence of fluorescence intensity on PS−PEG concentration was confirmed up to 0.06 mg/mL of DiR-loaded PS−PEG nanoparticles in a 6:3:1 by volume mixture of DMF, Triton X-100, and water. As described in detail in the Experimental Procedures section, the concentrations of DiR-loaded PS−PEG nanoparticles in organ tissue samples were measured using ethyl acetate/Triton X-100 extracts from tissue homogenates; the results of these measurements will be discussed in the next subsection. Using aqueous solutions containing known concentrations of DiR-loaded PS−PEG micelles, we found that this liquid−liquid extraction procedure involving the extraction of DiR by ethyl acetate/Triton X-100 gives an extraction efficiency of 61%. Therefore, when estimating the concentration of DiR-loaded PS−PEG nanoparticles in an organ tissue from the measured fluorescence intensity, a correction factor was applied to correct for the incomplete extraction of DiR. Also, of note, the upper concentration limit for the linear dependence of fluorescence intensity on PS−PEG concentration (Figure S5B) corresponds to about 29 μg of DiR-loaded PS−PEG nanoparticles per 0.2 g of the organ tissue. Therefore, as can be seen from Figures 3 and 4, the calibration covers a sufficient range of nanoparticle concentration values for the PK/BD study.

Pharmacokinetics (PK) and Biodistribution (BD) of PS−PEG Nanoparticles Following Pharyngeal Instillation in Mice. The concentrations of DiR-loaded PS−PEG nanoparticles in the lungs and other organs after pharyngeal aspiration in mice were measured as functions of time by ex vivo fluorescence imaging of the organs of interest excised from the mice. The fluorescent light emitted from DiR (λ_{em} = 790 nm) under 745 nm excitation has an optical penetration depth of ∼1 cm in tissues,[29] which enabled (semi)quantitation of nanoparticle contents in excised organs (all organs of interest had thickness dimensions of <1 cm), although such quantitation was not possible by whole-body imaging. Fluorescence images show that pharyngeally instilled PS−PEG nanoparticles were evenly distributed across the lungs, which indicates that the PS−PEG nanoparticles were successfully delivered to the deep alveolar regions of the lungs (Figure 2A). Throughout the experiment period of 8 weeks, DiR-loaded PS−PEG nanoparticles were predominantly located in the lungs, rather than in other organs (as discussed in detail later), at both nanoparticle dose concentrations tested (0.6 mg/mL (group 1) and 6.0 mg/mL (group 2)). A continuous decrease in lung fluorescence was observed at both concentrations (Figure 2B). We note that the fluorescence intensity estimated from an analysis of whole-organ images may not linearly correlate with the concentration of the fluorescence probe (DiR) because interparticle fluorescence self-quenching may reduce the quantum yield of DiR-loaded PS−PEG nanoparticles at high local nanoparticle concentrations[27] and also because the spatial distribution of the nanoparticles within an organ may vary as a function of nanoparticle concentration. To test whether this is indeed the case, DiR contents in whole-organ specimens were also analyzed using organic extracts from organ tissue homogenates prepared as described in the Experimental Procedures section.

https://doi.org/10.1021/acs.biomac.2c00221
Biomacromolecules 2022, 23, 2471−2484

DiR-loaded PS−PEG nanoparticle concentrations in the lungs, other excretory organs, blood, and feces of mice collected at different times after pharyngeal administration were determined (N = 4) using extracts of DiR/PS−PEG in ethyl acetate/Triton X-100 from tissue homogenates. Figure 3

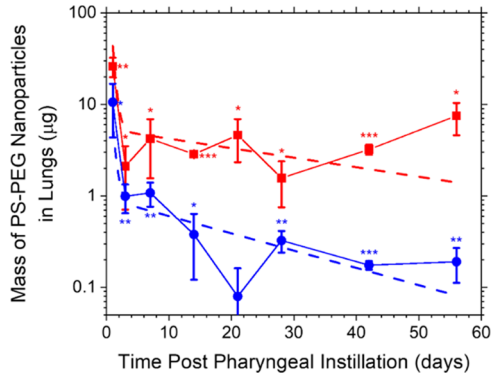

Figure 3. Average mass of DiR-loaded PS−PEG nanoparticles in the lungs ($N_{lung}(t)$) estimated from organic extracts from tissue homogenates of lung specimens collected at different times following pharyngeal instillation of the nanoparticles (N = 4, error bar = SD in linear scale). Statistical significance against control (fluorescence from the lungs measured 1 day after pristine PS−PEG nanoparticle instillation) was assessed by one-tailed Welch's t-test (*p <0.05, **p < 0.01, ***p < 0.001). The DiR-loaded PS−PEG nanoparticle dose concentrations used were the same as in Figure 2, i.e., 0.6 mg/mL for group 1 (blue/circles) and 6.0 mg/mL for group 2 (red/squares). Dashed lines are fits to the multicompartmental PK model ($N_{lung}(t) \cong N_{A,0}\, e^{-(k_A+k_T)t} + N_{B,0}\, e^{-k_B t}$, eq 4) to determine the values of the amounts (numbers of masses) of nanoparticles initially deposited in the alveoli and airways ($N_{A,0}$ and $N_{B,0}$, respectively) and the alveolar and airway clearance rate constants ($(k_A + k_T)$ and k_B, respectively).

displays the results obtained at the two different dose concentrations of DiR-loaded PS−PEG nanoparticles, i.e., 0.6 mg/mL (group 1) and 6.0 mg/mL (group 2). At all initial nanoparticle doses and measurement time points, the PS−PEG nanoparticle concentrations in the lungs were measured to be significantly higher than the lower detection limit (LDL) of the nanoparticles (0.07 μg per g of lung tissues estimated based on the background fluorescence of the lungs treated with non-DiR-loaded PS−PEG nanoparticles). The overall trends were similar between data shown in Figures 3 and 2B. However, the rapid decay in nanoparticle concentration at early time points (i.e., an order-of-magnitude decrease during the first 3 days) was clearly visible only in the data obtained with organic extracts (Figure 3); the whole-organ fluorescence showed a more gradual decrease over the entire measurement period (Figure 2B) likely due to increased fluorescence self-quenching at higher concentrations of DiR-loaded nanoparticles and also due to slower elimination (longer retention) of the nanoparticles deposited in the peripheral (i.e., alveolar) regions of the lungs (further discussed in the next subsection on PK modeling analysis). In mice treated with 0.6 mg/mL DiR-loaded PS−PEG nanoparticles (group 1), the nanoparticle concentration in the lungs appeared to continue to decrease even after day 3, whereas for mice treated with 6.0 mg/mL DiR-loaded nanoparticles (group 2), the decline in lung nanoparticle concentration at long times was less clear (Figure 3). In both cases (groups 1 and 2), the percentage of retention of the nanoparticles in the lungs relative to the amount administered reduced to a level of 10−20% within a day after administration (Figure S6), which suggests that a rapid clearance mechanism ("mucociliary escalator") is operative that efficiently removes nanoparticles from conducting airways.[30]

Figure 4 displays the masses of DiR-loaded PS−PEG nanoparticles detected in the liver, heart, kidneys, spleen, brain, and blood, normalized by the wet masses of the respective organs and blood. Among all secondary organs examined, the liver and spleen, which are rich in mononuclear phagocytes, showed relatively higher amounts of PS−PEG nanoparticles, which suggests that the nanoparticles are taken up by macrophages in the circulatory system (i.e., Kupffer cells in the liver sinusoids).[31] The kidneys and brain showed negligible traces of PS−PEG nanoparticles because the filtration thresholds of these organs are much smaller (~5.5 nm in diameter for the kidney's glomerular membrane[32] and ~400 Da in molecular weight for the blood−brain barrier[33]) than the size of the nanoparticles (32 nm in hydrodynamic diameter). Urine specimens were also collected using a filter paper for a 24 h period at different time points; as shown in Figure S7, no trace of nanoparticles (no fluorescence signal in the filter paper) was detected, which is consistent with the kidney data. Overall, the concentrations of nanoparticles detected in the secondary organs were 2−3 orders of magnitude lower than the concentration measured in the lungs at all times. This result suggests that translocation of PS−PEG nanoparticles into the systemic circulation occurs extremely slowly, which is also supported by low plasma concentrations of the nanoparticles (Figure 4). In all secondary organs and blood, the concentrations of PS−PEG nanoparticles dropped below the LDL of the nanoparticles (≅0.04 μg per g of the tissue) after ~14 days after instillation; the only exception was data obtained from the livers of mice in group 2, which showed a significant level of nanoparticle retention even up to 3−4 weeks.

Figure 5 shows the amounts of DiR-loaded PS−PEG nanoparticles detected in feces collected during a 24 h interval at different times from designated subgroups of mice within groups 1 and 2, which were sacrificed on day 56 (N = 4). On days 2−3, for instance, the daily amounts of DiR-loaded PS−PEG nanoparticles excreted in feces were 0.3 μg for group 1 and 7 μg for group 2, which exceed the respective total amounts accumulated in secondary organs and blood (0.05 μg for group 1 and 0.3 μg for group 2). Data shown in Figure S4, 3, and 4 suggest that DiR-loaded PS−PEG micelles are stable, and after pharyngeal instillation, they are rapidly cleared from the lungs, while they do not rapidly translocate into the circulation and other organs. Therefore, the combined results including the data in Figure 5 establish that pharyngeally instilled PS−PEG nanoparticles are initially cleared from the lungs and from the body predominantly by noncirculatory mechanisms, which likely involve the transport of the nanoparticles through the larynx, esophagus, stomach, and gastrointestinal tract (GIT), and excretion as undigested materials in feces.[34,35]

To determine the percentage of the instilled nanoparticles that were already lost to the esophagus from the beginning due to swallowing and/or coughing during the pharyngeal instillation procedure, additional experimentation was performed in which the distribution of instilled liquid was imaged by X-ray computed tomography (CT). Mice received a pharyngeal instillation of an NS solution containing pristine PS−PEG nanoparticles (0.6 mg/mL) along with a water-

https://doi.org/10.1021/acs.biomac.2c00221
Biomacromolecules 2022, 23, 2471−2484

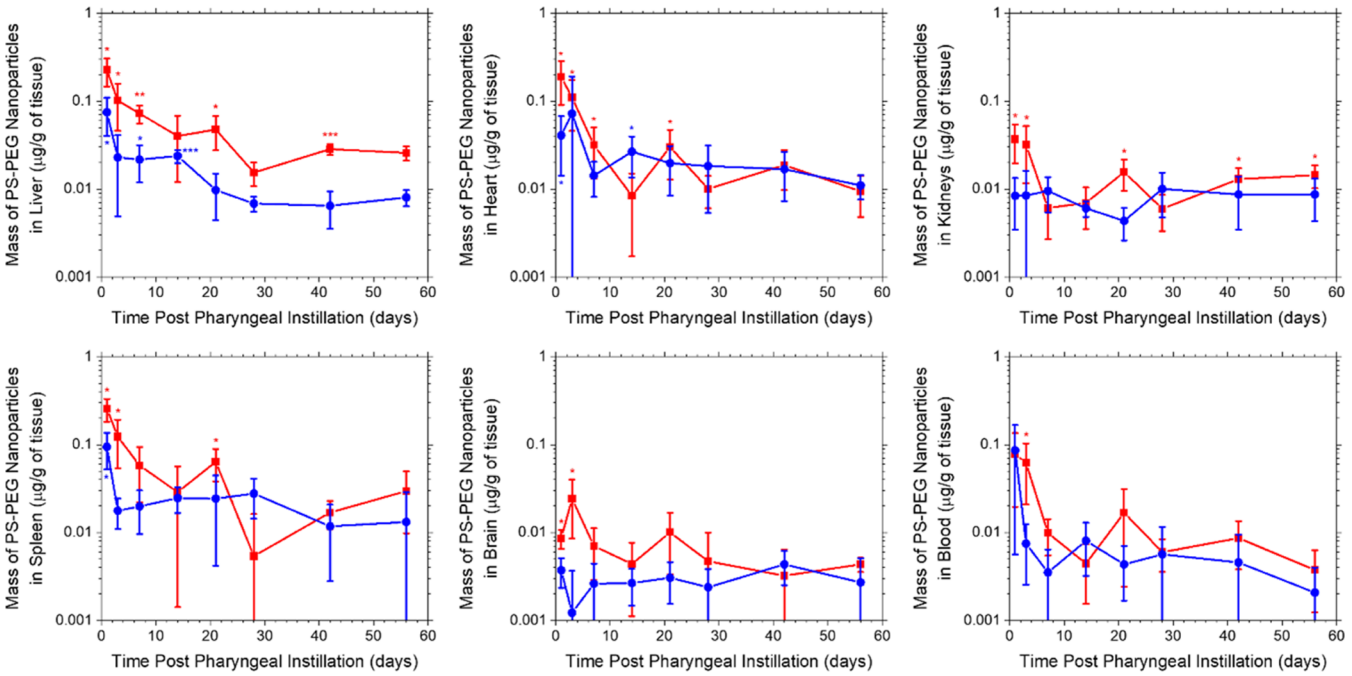

Figure 4. Average masses of DiR-loaded PS−PEG nanoparticles in the liver, heart, kidneys, spleen, brain, and blood, estimated from organic extracts from tissue homogenates of organ specimens collected at different times following pharyngeal instillation of the nanoparticles (N = 4, error bar = SD in the linear scale). The nanoparticle mass was normalized by the wet mass of the organ. Statistical significance against control (fluorescence from the respective organ measured 1 day after pristine PS−PEG nanoparticle instillation) was assessed by one-tailed Welch's t-test (*p < 0.05, **p < 0.01, ***p < 0.001). The DiR-loaded PS−PEG nanoparticle dose concentrations used were the same as in Figure 2, i.e., 0.6 mg/mL for group 1 (blue/circles) and 6.0 mg/mL for group 1 (red/squares).

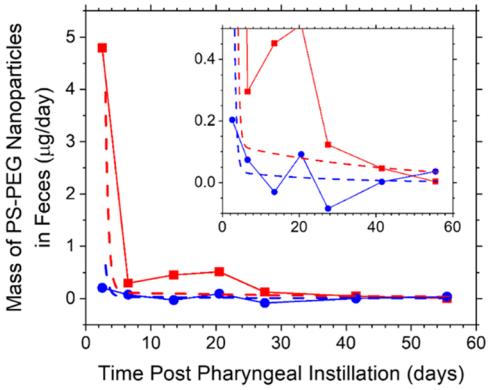

Figure 5. Average mass of DiR-loaded PS−PEG nanoparticles excreted in feces ($\Delta N_E(t)$) estimated from organic extracts from homogenates of feces specimens collected during a period at different times following pharyngeal instillation of the nanoparticles (N = 4, SD values not evaluated because each data point represents an aggregate of specimens from all four animals per cage). Nanoparticle mass was estimated using background-subtracted fluorescence data; the background fluorescence was obtained from mice treated with pristine PS−PEG nanoparticles. The DiR-loaded PS−PEG nanoparticle dose concentrations used were the same as in Figure 2, i.e., 0.6 mg/mL for group 1 (blue/circles) and 6.0 mg/mL for group 2 (red/squares). Dashed lines are fits to the multicompartmental PK model ($\Delta N_E(t) \cong N_{A,0}(e^{(k_A+k_T)\Delta t} - 1)e^{-(k_A+k_T)t} + N_{B,0}(e^{k_B\Delta t} - 1)e^{-k_B t}$ (where Δt = 24 h), eq 6) to determine the values of $N_{A,0}$, $N_{B,0}$, $(k_A + k_T)$, and k_B.

soluble X-ray contrast agent, Iohexol (50 mg I/mL). Immediately after instillation, the mice were scanned using a micro-CT scanner under isoflurane anesthesia. By analysis of micro-CT images (Figure 6), it was determined that only about 27% of the instilled liquid volume was initially detected in the esophagus region of the digestive tract, which is consistent with a previous report (~12−23% of liquid not delivered to the lungs after pharyngeal administration).[36] This result confirms that the majority (~73%) of the nanoparticle dose was properly delivered to the pulmonary system at the beginning.

Analysis Based on a Multicompartmental PK Model. As shown in Figures 2−5, pharyngeally instilled PS−PEG nanoparticles were cleared from the lungs in two phases (a rapid phase during the first 2−3 days followed by a slow phase occurring over a period of several weeks), and the nanoparticles cleared from the lungs were detected at multiple locations in the body, particularly, in the circulatory and excretory systems (blood, liver, spleen, and feces). These results suggest that the transport of pharyngeally instilled PS−PEG nanoparticles involves multiple mechanisms, which include the action of the mucociliary escalator,[30] phagocytosis by alveolar macrophages,[37] passive translocation through the BAB or the lymphatic epithelium,[10,38] and hepatobiliary clearance through the liver.[39] To quantitatively analyze the data shown in Figures 3 and 5, a multicompartmental PK model was developed that takes into account all of the nanoparticle clearance pathways mentioned above (Figure 7). Although several more sophisticated, physiologically based pulmonary clearance models have previously been proposed for inhaled biopersistent nanoparticles,[13,14] the first-order kinetic equations were assumed for all steps within our model because such a level of description is sufficient for our purpose of determining relative roles of different nanoparticle clearance mechanisms. For a kinetic description of the clearance process, the lung system was described as being composed of two subcompartments: (i) the conducting airways (including the trachea, bronchi, and bronchioles) in

https://doi.org/10.1021/acs.biomac.2c00221
Biomacromolecules 2022, 23, 2471−2484

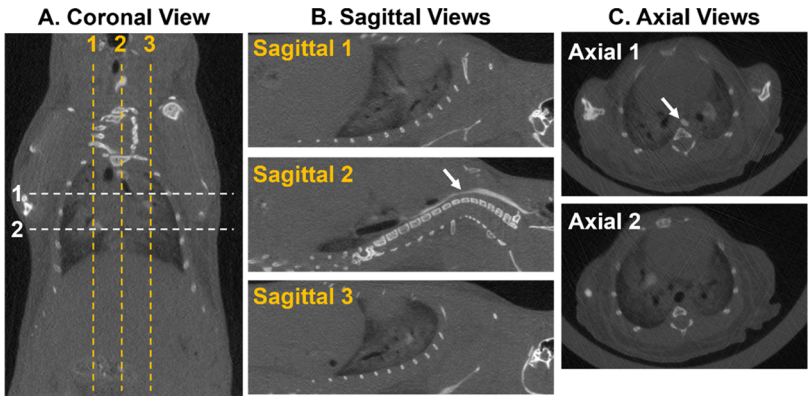

Figure 6. Micro-CT cross sectional images (N = 1) of the mouse torso immediately after pharyngeal administration of a solution containing PS−PEG nanoparticles and Iohexol, which is a water-soluble CT contrast agent. (A) Coronal, (B) sagittal, and (C) axial views, where the locations of cross sections are indicated as dashed lines in (A). Arrows on the bright regions indicate the location of the esophagus.

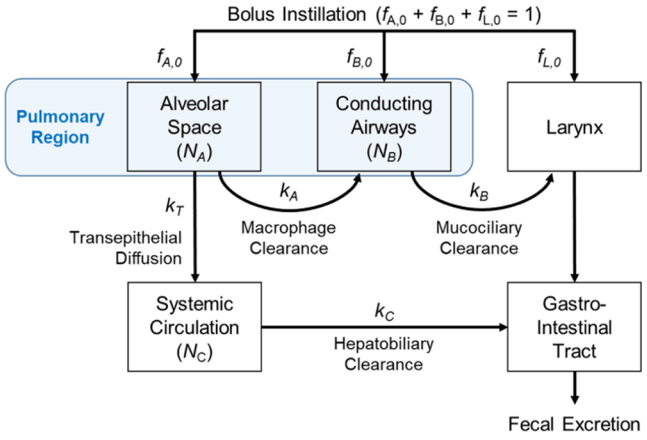

Figure 7. Multicompartmental PK model describing pulmonary compartments and pathways associated with the clearance of pharyngeally instilled PS−PEG nanoparticles. $f_{A,0}$, $f_{B,0}$, and $f_{L,0}$ denote the fractions of the instilled PS−PEG nanoparticles initially deposited in the alveolar space, conducting airways, and larynx, respectively. N_A, N_B, and N_C denote the numbers of the PS−PEG nanoparticles remaining in the alveolar space, conducting airways, and systemic circulation, respectively; N_A, N_B, and N_C are time-dependent quantities. PS−PEG nanoparticles are assumed to be biopersistent; they neither degrade chemically or biologically, nor form aggregates themselves or with biological molecules.

which the mucociliary clearance of nanoparticles takes place and (ii) the alveoli where nanoparticles are taken up by alveolar macrophages and delivered to the airways or pass into the capillary blood/lymph nodes by transepithelial diffusion.[12,40] Chemical degradation or physical dissociation of PS−PEG nanoparticles was not considered in the model because PS−PEG is a chemically stable polymer and also PS−PEG nanoparticles (micelles) are kinetically frozen structures; the glass transition temperature (T_g) of the PS core domain has been measured to be ∼61 °C (unpublished result), and therefore, even in the presence of biological amphiphiles (such as bile acids in the small intestine), it is unlikely that PS−PEG nanoparticles will undergo dissociation and release DiR molecules. Urinary clearance was not included for the reason discussed in the previous subsection. Gastrointestinal resorption of the nanoparticles was also neglected because the extent of intestinal absorption has been reported to be <1% for similarly sized nanoparticles.[41,42] The detailed kinetic mass balance equations for nanoparticles in different tissue compartments and analytical solutions to those equations (i.e., biexponential functions for the nanoparticle contents in the lungs and feces) are presented in the Theoretical Model & Analysis Procedures section.

The time-dependent nanoparticle concentration profiles in the lungs (Figure 3) and feces (Figure 5) were simultaneously fit to this multicompartmental PK model (i.e., eq 4 ($N_{lung}(t) \cong N_{A,0}\, e^{-(k_A+k_T)t} + N_{B,0}\, e^{-k_B t}$) and eq 6 ($\Delta N_E(t) \cong N_{A,0}(e^{(k_A+k_T)\Delta t} - 1)e^{-(k_A+k_T)t} + N_{B,0}(e^{k_B \Delta t} - 1)e^{-k_B t}$)). As discussed in the previous subsection, about 27% of pharyngeally instilled PS−PEG nanoparticles were initially lost to the esophagus ($f_{L,0}$ = 0.27, determined by a micro-CT scan (Figure 6)). Therefore, in the fitting analysis, the initial fraction of PS−PEG nanoparticles delivered to the pulmonary system was fixed at 73% (i.e., $f_{A,0} + f_{B,0}$ (= $1 - f_{L,0}$) = 0.73). As described in detail in the Theoretical Model & Analysis Procedures section, four adjustable parameters were used in the least-square fits of the experimental data; they are $N_{A,0}$, $N_{B,0}$, ($k_A + k_T$), and k_B, and their definitions are given in Figure 7. The best-fit results are summarized in Table 1. As shown in Figures 3 and 5, the kinetics of lung clearance and fecal excretion of the nanoparticles could be reasonably described using the biexponential decay functions. As shown in Table 1, the rate constant associated with the airway clearance process (k_B) is at least about two orders of magnitude higher than those associated with the alveolar clearance processes ($k_A + k_T$), which confirms that the clearance of nanoparticles from the conducting airways due to the mucociliary escalator is far faster than the clearance of nanoparticles from the alveolar space due to uptake by macrophages (k_A) or transepithelial diffusion into the circulation either directly or via the lymph (k_T).[37] As a result, the time-dependent nanoparticle concentration profile in the lung tissue shows two distinct phases of clearance (Figure 3), i.e., a fast clearance phase (at t <3 days) due to the mucociliary clearance followed by a slower phase (at longer times) due to the alveolar clearance processes.[43]

The half-lives of the mucociliary and alveolar clearance processes were estimated to be $t_{1/2,B}$ = 0.36 ± 0.13 days and $t_{1/2,A}$ = 16 ± 4 days, respectively, for instance, when 80 μL of a DiR-loaded PS−PEG nanoparticle suspension was pharyngeally instilled at a nanoparticle dose concentration of 0.6 mg/mL; the rate of nanoparticle clearance by the mucociliary escalator is about 40 times faster than the rate at which the nanoparticles are eliminated from the alveolar space by macrophage uptake and diffusion. The estimated timescale

https://doi.org/10.1021/acs.biomac.2c00221
Biomacromolecules 2022, 23, 2471−2484

for mucociliary clearance is in good agreement with values reported in the literature (i.e., <2 days for nanoparticles in rodents).[9,30,44] The timescale for nanoparticle clearance in the alveoli is known to vary widely, from ∼1 hour to ∼100 days, depending on the size and surface chemistry of the nanoparticles.[10,45] Nevertheless, our result appears to be in a reasonable agreement with the literature, considering the specific characteristics of PS−PEG nanoparticles used in this study (further discussed later). Notably, PS−PEG nanoparticles were found to remain in the alveolar region, which is the site of therapeutic action of the nanoparticles, for >2 weeks. However, the actual fraction of PS−PEG nanoparticles initially deposited in the alveoli (i.e., the bioavailability of the nanoparticles) was found to be low (e.g., $f_{A,0} = 0.019 \pm 0.009$ for group 1). Most of the administered dose was sequestered in the airways ($f_{B,0} = 0.71 \pm 0.01$) because a plug of liquid passing through the airways typically leaves a trailing film on the walls of the airways; the amount of liquid lost to the airway walls ("coating cost") can be reduced by increasing the liquid injection rate.[46] In our "tongue-pull" procedure, a plug of liquid formed in the larynx is pulled into the trachea by natural inhalation, and therefore, the rate of liquid injection is slower than in pressurized situations.[30,47]

It was also possible to quantitatively fit the whole-organ lung fluorescence radiance profiles in Figure 2B with a similar double-exponential decay function ($I(t) = I_{A,0}\, e^{-(k_A+k_T)t} + I_{B,0}\, e^{-k_B t}$, eq 9) using $I_{A,0}$ and $I_{B,0}$ as fitting parameters; the values for the alveolar and airway clearance rate constants (i.e., $(k_A + k_T)$ and k_B, respectively) were kept the same as the values obtained previously by fitting the data in Figures 3 and 5 to the multicompartmental PK model. From the best-fit values of $I_{A,0}$ and $I_{B,0}$ (Table 1), the intensity-weighted values of $N_{A,0}$ and $N_{B,0}$ (Table 1) were estimated, respectively, using the correlation between the fluorescence count rate (I) from an excised entire lung specimen and the mass of DiR-loaded PS−PEG nanoparticles in the lungs estimated from an organic extract from a tissue homogenate of the lung specimen shown in Figure S8; the intensity-weighted values of $f_{A,0}$ and $f_{B,0}$ (Table 1) were also calculated using their definitions, $f_{A,0} = N_{A,0}/N_0$ and $f_{B,0} = N_{B,0}/N_0$, where $N_0 = 48\ \mu g$ (group 1) and 480 μg (group 2). Interestingly, the value of the ratio $f_{A,0}/f_{B,0}$ estimated from the whole-organ fluorescence data ($f_{A,0}/f_{B,0} = 0.28$ at the nanoparticle dose concentration of 0.6 mg/mL) was an order of magnitude greater than measured using the extraction procedure ($f_{A,0}/f_{B,0} = 0.027$ at the same nanoparticle dose concentration) (Table 1). There are two possible reasons for this: (i) because of interparticle fluorescence self-quenching between DiR-loaded PS−PEG nanoparticles, the whole-organ fluorescence of the lungs was not proportionally high at higher local nanoparticle concentrations and (ii) the fluorescence intensity estimated from a whole lung image was dominated by nanoparticles located in the distal (i.e., alveolar) regions of the lungs, while the nanoparticles in the distal zones were cleared slower.

Data fitting was less accurate for group 2 because of large errors at long times. At the nanoparticle dose concentration of 6.0 mg/mL (group 2), the alveolar half-life was almost twice as large ($t_{1/2,A} = 29 \pm 20$ days, estimated by fitting data in Figures 3 and 5 to the multicompartmental PK mode) as that at 0.6 mg/mL (group 1) ($t_{1/2,A} = 16 \pm 4$ days), which is attributed to the saturation of the phagocytic capacity of alveolar macrophages in the higher nanoparticle dose situation, as will be discussed in the Discussion section. As shown in Figure 2B, for group 2, the fluorescence radiance (red squares in Figure 2B) showed a slower decay than estimated based on the fitting analysis of data in Figures 3 and 5 (red dotted line in Figure 2B), which, again, might suggest that nanoparticles located in the peripheral (alveolar) regions make dominant contributions to the overall fluorescence intensity, although increased fluorescence quenching with increasing nanoparticle concentration might also have contributed to this behavior. The half-lives of nanoparticles in the airways were comparable between group 1 ($t_{1/2,B} = 0.36 \pm 0.13$ days) and group 2 ($t_{1/2,B} = 0.32 \pm 0.03$ days); the kinetics of mucociliary clearance was unaffected by nanoparticle dose concentration. For group 2, the fraction of nanoparticles reaching the alveoli upon instillation ($f_{A,0} = 0.011 \pm 0.003$) was lower by about 42% than that for group 1 ($f_{A,0} = 0.019 \pm 0.007$), likely because the coating loss was increased when the liquid's viscosity was increased and the liquid's surface tension was decreased at the increased concentration of the nanoparticles.[48]

DISCUSSION

Delivery and Bioavailability of PS−PEG Nanoparticles in the Alveolar Space. Pharyngeal aspiration was employed to deliver PS−PEG nanoparticles into the alveolar airspace. Pharyngeal aspiration is a noninvasive procedure that is simple to implement and is a reasonable mimic of the intratracheal instillation procedure used in the clinic.[16,40] Pharyngeal aspiration provided a seemingly homogeneous distribution of PS−PEG nanoparticles to the alveoli (Figure 2A), although the bioavailability of the nanoparticles in the alveoli was somewhat low (1−2% relative to the total amount administered). Pharyngeal aspiration involves multiple steps, including the initial loading of liquid at the pharynx, the penetration of the liquid into the larynx, the inhalation of the liquid into the trachea, etc. However, during this process, the oto-respiratory reflex of the mouse causes the loss of some amount of liquid. Unlike the clinical intratracheal instillation procedure (which involves an intubation of the trachea followed by instillation of liquid and thus enables delivery of liquid into the trachea without loss), pharyngeal aspiration typically delivers only ∼80% of the loaded liquid into the trachea.[36] In our micro-CT experiment, about 27% of the administered liquid was detected in the GIT, particularly in the esophagus, immediately after pharyngeal instillation (Figure 6), which is consistent with the previous literature. It is known that pharyngeal/intratracheal instillation often produces an uneven distribution of the administered liquid across the lung,[49] because the liquid is transported through the airways as a plug.[48] Our analysis indicates that about 1−2% of the administered PS−PEG nanoparticles were delivered to the alveoli. This result is consistent with what has previously been reported in the literature; Kazemi et al. reported an alveolar delivery efficiency of 4.7% for intratracheal liquid instillation of surfactant at a dose volume of 1 mL/kg in rats.[46] However, it would be beneficial to try to further improve the alveolar delivery efficiency of PS−PEG nanoparticles in the future, for instance, by increasing the liquid injection volume,[48] to enhance the bioavailability of the polymers in the alveolar regions.

Retention of PS−PEG Nanoparticles in the Alveolar Regions. The alveolar retention time of nanoparticles is influenced by particle size and surface chemistry because they affect the rates of phagocytosis and diffusion through the BAB and lymph.[12,50] The uptake of nanoparticles by alveolar macrophages becomes less efficient at sizes smaller than about

https://doi.org/10.1021/acs.biomac.2c00221
Biomacromolecules 2022, 23, 2471−2484

100 nm.[38] Surface functionalization of nanoparticles with PEG chains also reduces their recognition and subsequent uptake by macrophages because the PEG functionalization ("PEGylation") prohibits the adsorption of opsonin proteins to the surfaces of the nanoparticles.[51] On the other hand, small PEGylated nanoparticles are efficient at translocating through epithelial cells[44] and thus through the BAB and lymphatic vessel.[10,52,53] Therefore, it is reasonable to expect that PS−PEG nanoparticles having a diameter of ∼32 nm are cleared from the alveoli mainly by the transepithelial diffusion mechanism, although the extent of phagocytosis cannot be completely ignored as evidenced for other PEGylated nanoparticles.[37,54] Also, uptake and trafficking of nanoparticles by dendritic cells to lymphatic vessels are known to increase with reducing size and PEG functionalization of nanoparticles.[12,55]

The two mouse cohorts treated at two different nanoparticle dose concentrations (groups 1 and 2) exhibited significantly different lung clearance profiles of the nanoparticles at long times. At the low nanoparticle dose concentration tested (0.6 mg/mL, group 1), the concentration of PS−PEG nanoparticles in the lungs (i.e., in the alveoli) continuously decreased following first-order kinetics. The alveolar half-life of the PS−PEG nanoparticles (∼2 weeks) is significantly shorter than the half-life values reported for non-PEGylated 7 nm diameter cerium nanoparticles (103 days)[45] and non-PEGylated 50 nm diameter titanium nanoparticles (∼28 days),[43] which is understandable in that these non-PEGylated nanoparticles must have existed as large aggregates.[12] However, at the 10× nanoparticle dose concentration (6.0 mg/mL, group 2), the nanoparticle concentration in the lungs remained almost unchanged over the 2-month test period. The alveolar clearance rate constant estimated for group 2 ($(k_A + k_T) = 0.024 \pm 0.016\ \text{day}^{-1}$) was about half of that for group 1 ($(k_A + k_T) = 0.043 \pm 0.010\ \text{day}^{-1}$). This result is consistent with the previous report that alveolar phagocytosis of nanoparticles is a saturable process in which the rate constant for nanoparticle clearance (k_A) decreases with increasing nanoparticle load;[14] for this reason, the Michaelis−Menten kinetics, for instance, has been used for describing the rates of phagocytic clearance of nanoparticles.[14] Taken together, both the phagocytosis and transepithelial diffusion mechanisms are operative in the alveolar clearance of PS−PEG nanoparticles. The bioavailability of PS−PEG nanoparticles within the alveoli (AUC_A, estimated using eq 7b) was fortuitously observed to scale linearly with nanoparticle dose concentration (Table 1); relative to group 1, group 2 showed a lower efficiency of the delivery of nanoparticles and a longer retention of nanoparticles in the alveoli, and these two effects of higher-dose nanoparticles appear to have been canceled out.

Entrapment of PS−PEG Nanoparticles in the Airways. The mucus layer in the airways has a mesh size of ∼300 nm and is also covered with lung surfactants.[56] Therefore, PS−PEG nanoparticles (∼32 nm) are likely to penetrate the mucus gel and reach the underlining periciliary layer. Schneider et al. have shown that PS−PEG nanoparticles smaller than 300 nm can reach the periciliary layer and airway epithelium and thus exhibit a longer retention time (<∼1 day) in the airways than larger nanoparticles that cannot penetrate the mucus layer.[44] However, small nanoparticles can also diffuse back into the mucus layer from the underlying tissue, and therefore, the rate of nanoparticle clearance from the airways is still expected to be faster than that from the alveoli; as shown in Table 1, the alveolar half-life of PS−PEG nanoparticles was about 2 weeks, which is much longer than the airway residence time of small PS−PEG nanoparticles reported in the literature (<∼1 day).[44]

In theory, it is possible to add an additional compartment representing the periciliary layer/airway epithelium and accordingly additional kinetic steps associated with the entrapment of nanoparticles within that compartment in the multicompartmental PK model. However, this modification was not attempted in the present study because it would significantly reduce the accuracy of the fitting process.

Toxicological Effects of PS−PEG Nanoparticles. Synthetic nanoparticles may induce inflammatory responses in the alveoli. Longer retention increases the chances of such a situation. Further, translocation of nanoparticles into the circulation and their accumulation in secondary organs may cause systemic toxicity. We found that only small percentages (1−2%) of the administered PS−PEG nanoparticles were able to reach the alveolar regions, and those nanoparticles deposited in the alveoli remained therein for >2 weeks. It is possible that some amount of PS−PEG nanoparticles are trapped within the alveolar epithelial layer and internalized by dendritic cells,[44,53] which may respectively lead to dysfunction of epithelial cell metabolism and activation of immune responses upon trafficking to the lymphatic system. Previously, similar nanoparticles (noncharged PS nanoparticles of 60 nm diameter) have been shown to not elicit any significant inflammatory responses (e.g., activation of neutrophils and lymphocytes and increased cytokine levels) in the lungs of hamsters.[57] However, this previous investigation only focused on acute/short-term effects of the nanoparticles (at t = 1 h), and longer-term toxicological studies (over >1 day) have not been reported. Long-term toxicological effects of PS−PEG nanoparticles, including detailed immune responses (pro/anti-inflammatory cytokine profiles, immune cell phenotypes, etc.), will need to be studied in the future.

In the high-dosed group (group 2, treated at a nanoparticle dose concentration of 6.0 mg/mL), a small percentage (1−2%) of the instilled PS−PEG nanoparticles persisted in the lungs even beyond the eight-week measurement period. We would like to note that at the dose volume used (4.0 mL/kg body weight), the 0.6 and 6.0 mg/mL nanoparticle dose concentrations correspond to, respectively, 1× and 10× the optimal therapeutic dose identified in our previous study.[8] In other words, the high dose concentration tested (which corresponds to 10× the therapeutic dose) will not likely be used in real clinical settings. Nevertheless, it is possible that the FDA will require that the IND-enabling study design includes an assessment of chronic/long-term (>2 months) toxicological hazards following excessive doses (>10× the therapeutic dose) of PS−PEG nanoparticles. We plan on performing these experiments in the future. However, exploration of this topic is outside the scope of our current study.

In a previous publication, we have reported that PS−PEG nanoparticles at doses up to 6 mg per mouse (1−2 orders of magnitude greater than the doses used in this work) do not cause any damage to the alveolar tissue or affect the cytokine response in the lungs of mice (based on analysis of histological sections and bronchoalveolar lavage (BAL) fluid samples at 7 days after pharyngeal administration of the nanoparticles).[8] In the present study, all mice treated with PS−PEG nanoparticles were confirmed to remain healthy, showing normal respiration, a steady growth in body weight, and a stable lung weight throughout the 2-month study period (Figure S9). No significant accumulation of PS−PEG nanoparticles in other

https://doi.org/10.1021/acs.biomac.2c00221
Biomacromolecules 2022, 23, 2471−2484

organs and blood was detected after 2 weeks after administration, except for the liver, which is the major mononuclear phagocyte system for clearance of foreign substances from the circulation. Previous mouse studies have shown that intravenous and oral administrations of small PEGylated nanoparticles do not induce any significant toxicity in the liver.[58,59] Possible effects of PS−PEG nanoparticles on the intestine's function will need to be investigated because the majority of the nanoparticles are cleared through the GIT due to the initial spillover of the instilled liquid into the esophagus and also the clearance of the nanoparticles by the mucociliary escalator.[58]

CONCLUSIONS

In summary, the pharmacokinetic and biodistribution properties of a novel polymer lung surfactant (PLS) formulation (namely, PS−PEG micelle nanoparticles) were evaluated over a 2-month period of time following pharyngeal administration in mice. The time-dependent lung retention profiles of PS−PEG nanoparticles showed biphasic clearance rates: a fast mucociliary escalator process occurring in the conducting airways and a much slower alveolar clearance process involving a combination of the phagocytic action of macrophages and direct nanoparticle translocation through the blood−air barrier (BAB) or the lymphatic epithelium. Pharyngeally administered PS−PEG nanoparticles were mainly excreted as feces. The elimination half-life of PS−PEG nanoparticles from the alveoli depended upon nanoparticle dose concentration, presumably because of the saturable nature of the clearance of nanoparticles by macrophages in the alveoli. Nanoparticle accumulation in secondary organs was not significant except in the liver where hepatobiliary clearance occurs. Although detailed toxicological evaluations remain to be done, no primary symptoms of toxicity were observed in mice treated with PS−PEG nanoparticles. The "tongue-pull" pharyngeal nanoparticle instillation procedure was only able to provide a low efficiency of the delivery of PS−PEG nanoparticles to the site of therapeutic action, i.e., the alveoli. Further studies are warranted specifically to address the need for improving the delivery efficiency/bioavailability and also for understanding the detailed long-term toxicological effects of PS−PEG nanoparticles.

ASSOCIATED CONTENT

Supporting Information

The Supporting Information is available free of charge at https://pubs.acs.org/doi/10.1021/acs.biomac.2c00221.

NMR (Figure S1) and GPC (Figure S2) of PS−PEG; surface pressure−area isotherms (Figure S3) and time (Figure S4) and concentration (Figure S5) dependences of fluorescence intensities of DiR-loaded PS−PEG nanoparticles; lung retention of DiR-loaded PS−PEG nanoparticles (Figure S6); urine excretion of DiR-loaded PS−PEG nanoparticles (Figure S7); correlation between whole-organ fluorescence vs. DiR-loaded PS−PEG nanoparticle mass in the lungs (Figure S8); mouse body and lung weights as functions of time (Figure S9) (PDF)

AUTHOR INFORMATION

Corresponding Author

You-Yeon Won − *Davidson School of Chemical Engineering, Purdue University, West Lafayette, Indiana 47907, United States; Purdue University Center for Cancer Research, Purdue University, West Lafayette, Indiana 47907, United States;* orcid.org/0000-0002-8347-6375; Phone: +1-765-494-4077; Email: yywon@purdue.edu; Fax: +1-765-494-0805

Authors

Seyoung Kim − *Davidson School of Chemical Engineering, Purdue University, West Lafayette, Indiana 47907, United States*

Daniel J. Fesenmeier − *Davidson School of Chemical Engineering, Purdue University, West Lafayette, Indiana 47907, United States*

Sungwan Park − *Davidson School of Chemical Engineering, Purdue University, West Lafayette, Indiana 47907, United States*

Sandra E. Torregrosa-Allen − *Purdue University Center for Cancer Research, Purdue University, West Lafayette, Indiana 47907, United States*

Bennett D. Elzey − *Purdue University Center for Cancer Research, Purdue University, West Lafayette, Indiana 47907, United States*

Complete contact information is available at: https://pubs.acs.org/10.1021/acs.biomac.2c00221

Notes

The authors declare the following competing financial interest(s): A company, Spirrow Therapeutics, is currently attempting to commercialize the technology discussed in this manuscript. Y.Y.W. has an ownership interest in this company. A company, Spirrow Therapeutics, is currently attempting to commercialize the technology discussed in this manuscript. Y.Y.W. has an ownership interest in this company.

ACKNOWLEDGMENTS

The authors are grateful for funding from NSF (IIP-2036125) and Spirrow Therapeutics. The authors also acknowledge support from the Purdue University Center for Cancer Research (PCCR) via an NIH NCI grant (P30 CA023168), which supports the campus-wide NMR shared resources that were utilized in this work. Heidi Cervantes and Haley Harper at the Biological Evaluation Shared Resource (BE-SR) facility of PCCR are thanked for their technical assistance with the mouse studies.

REFERENCES

(1) Ranieri, V. M.; Rubenfeld, G. D.; Thompson, B. T.; Ferguson, N. D.; Caldwell, E.; Fan, E.; Camporota, L.; Slutsky, A. S. Acute Respiratory Distress Syndrome. *JAMA* **2012**, *307*, 2526−2533.

(2) Kim, H. C.; Won, Y.-Y. Clinical, Technological, and Economic Issues Associated with Developing New Lung Surfactant Therapeutics. *Biotechnol. Adv.* **2018**, *36*, 1185−1193.

(3) Guan, W.-j.; Ni, Z.; Hu, Y.; Liang, W.; Ou, C.; He, J.; Liu, L.; Shan, H.; Lei, C.; Hui, D. S. C.; Du, B.; Li, L.; Zeng, G.; Yuen, K.-Y.; Chen, R.; Tang, C.; Wang, T.; Chen, P.; Xiang, J.; Li, S.; Wang, J.; Liang, Z.; Peng, Y.; Wei, L.; Liu, Y.; Hu, Y.; Peng, P.; Wang, J.; Liu, J.; Chen, Z.; Li, G.; Zheng, Z.; Qiu, S.; Luo, J.; Ye, C.; Zhu, S.; Zhong, N. Clinical Characteristics of Coronavirus Disease 2019 in China. *N. Engl. J. Med.* **2020**, *382*, 1708−1720.

(4) Gattinoni, L.; Chiumello, D.; Rossi, S. COVID-19 Pneumonia: ARDS or Not? *Crit. Care* **2020**, *24*, 1−3.

(5) Willson, D. F.; Notter, R. H. The Future of Exogenous Surfactant Therapy. *Respir. Care* **2011**, *56*, 1369−1388.
(6) Raghavendran, K.; Willson, D.; Notter, R. H. Surfactant Therapy for Acute Lung Injury and Acute Respiratory Distress Syndrome. *Crit. Care Clin.* **2011**, *27*, 525−559.
(7) Piva, S.; DiBlasi, R. M.; Slee, A. E.; Jobe, A. H.; Roccaro, A. M.; Filippini, M.; Latronico, N.; Bertoni, M.; Marshall, J. C.; Portman, M. A. Surfactant Therapy for COVID-19 Related ARDS: A Retrospective Case−Control Pilot Study. *Respir. Res.* **2021**, *22*, 1−8.
(8) Kim, H. C.; Suresh, M. V.; Singh, V. V.; Arick, D. Q.; Machado-Aranda, D. A.; Raghavendran, K.; Won, Y.-Y. Polymer Lung Surfactants. *ACS Appl. Bio Mater.* **2018**, *1*, 581−592.
(9) Lipka, J.; Semmler-Behnke, M.; Sperling, R. A.; Wenk, A.; Takenaka, S.; Schleh, C.; Kissel, T.; Parak, W. J.; Kreyling, W. G. Biodistribution of PEG-Modified Gold Nanoparticles Following Intratracheal Instillation and Intravenous Injection. *Biomaterials* **2010**, *31*, 6574−6581.
(10) Choi, H. S.; Ashitate, Y.; Lee, J. H.; Kim, S. H.; Matsui, A.; Insin, N.; Bawendi, M. G.; Semmler-Behnke, M.; Frangioni, J. V.; Tsuda, A. Rapid Translocation of Nanoparticles from the Lung Airspaces to the Body. *Nat. Biotechnol.* **2010**, *28*, 1300−1303.
(11) Gill, K. K.; Nazzal, S.; Kaddoumi, A. Paclitaxel Loaded PEG5000−DSPE Micelles as Pulmonary Delivery Platform: Formulation Characterization, Tissue Distribution, Plasma Pharmacokinetics, and Toxicological Evaluation. *Eur. J. Pharm. Biopharm.* **2011**, *79*, 276−284.
(12) Liu, Q.; Guan, J.; Qin, L.; Zhang, X.; Mao, S. Physicochemical Properties Affecting the Fate of Nanoparticles in Pulmonary Drug Delivery. *Drug Discovery Today* **2020**, *25*, 150−159.
(13) Borghardt, J. M.; Weber, B.; Staab, A.; Kloft, C. Pharmacometric Models for Characterizing the Pharmacokinetics of Orally Inhaled Drugs. *AAPS J.* **2015**, *17*, 853−870.
(14) Stöber, W.; McClellan, R. O. Pulmonary Retention and Clearance of Inhaled Biopersistent Aerosol Particles: Data-Reducing Interpolation Models and Models of Physiologically Based Systems: - A Review of Recent Progress and Remaining Problems. *Crit. Rev. Toxicol.* **1997**, *27*, 539−598.
(15) Saad, W. S.; Prud'Homme, R. K. Principles of Nanoparticle Formation by Flash Nanoprecipitation. *Nano Today* **2016**, *11*, 212−227.
(16) Nielsen, T. B.; Yan, J.; Luna, B.; Spellberg, B. Murine Oropharyngeal Aspiration Model of Ventilator-Associated and Hospital-Acquired Bacterial Pneumonia. *J. Vis. Exp.* **2018**, *2018*, No. e57672.
(17) Borghardt, J. M.; Kloft, C.; Sharma, A. Inhaled Therapy in Respiratory Disease: The Complex Interplay of Pulmonary Kinetic Processes. *Can. Respir. J.* **2018**, *2018*, No. 2732017.
(18) Hitzman, C. J.; Wattenberg, L. W.; Wiedmann, T. S. Pharmacokinetics of 5-Fluorouracil in the Hamster Following Inhalation Delivery of Lipid-Coated Nanoparticles. *J. Pharm. Sci.* **2006**, *95*, 1196−1211.
(19) Pang, Y.; Sakagami, M.; Byron, P. R. The Pharmacokinetics of Pulmonary Insulin in the in Vitro Isolated Perfused Rat Lung: Implications of Metabolism and Regional Deposition. *Eur. J. Pharm. Sci.* **2005**, *25*, 369−378.
(20) Bachler, G.; Losert, S.; Umehara, Y.; von Goetz, N.; Rodriguez-Lorenzo, L.; Petri-Fink, A.; Rothen-Rutishauser, B.; Hungerbuehler, K. Translocation of Gold Nanoparticles across the Lung Epithelial Tissue Barrier: Combining in Vitro and in Silico Methods to Substitute in Vivo Experiments. *Part. Fibre Toxicol.* **2015**, *12*, 1−18.
(21) Bachler, G.; von Goetz, N.; Hungerbuhler, K. Using Physiologically Based Pharmacokinetic (PBPK) Modeling for Dietary Risk Assessment of Titanium Dioxide (TiO_2) Nanoparticles. *Nanotoxicology* **2015**, *9*, 373−380.
(22) Zhang, Y.-N.; Poon, W.; Tavares, A. J.; McGilvray, I. D.; Chan, W. C. W. Nanoparticle−Liver Interactions: Cellular Uptake and Hepatobiliary Elimination. *J. Controlled Release* **2016**, *240*, 332−348.
(23) Fesenmeier, D. J.; Park, S.; Kim, S.; Won, Y.-Y. Surface mechanical behavior of water-spread poly(styrene)−poly(ethylene glycol) (PS−PEG) micelles at the air−water interface: Effect of micelle size and polymer end/linking group chemistry. *J. Colloid Interface Sci.* **2022**, *617*, 764−777.
(24) Zhu, Z. Flash Nanoprecipitation: Prediction and Enhancement of Particle Stability via Drug Structure. *Mol. Pharmaceutics* **2014**, *11*, 776−786.
(25) Qian, J.; Berkland, C. Drug Release Kinetics from Non-degradable Hydrophobic Polymers Can Be Modulated and Predicted by the Glass Transition Temperature. *Adv. Healthcare Mater.* **2021**, *10*, No. 2100015.
(26) Park, K.; Otte, A.; Sharifi, F.; Garner, J.; Skidmore, S.; Park, H.; Jhon, Y. K.; Qin, B.; Wang, Y. Potential Roles of the Glass Transition Temperature of PLGA Microparticles in Drug Release Kinetics. *Mol. Pharmaceutics* **2021**, *18*, 18−32.
(27) Meng, F.; Wang, J.; Ping, Q.; Yeo, Y. Quantitative Assessment of Nanoparticle Biodistribution by Fluorescence Imaging, Revisited. *ACS Nano* **2018**, *12*, 6458−6468.
(28) Riehl, M.; Harms, M.; Göttel, B.; Kubas, H.; Schiroky, D.; Mäder, K. Acid-Induced Degradation of Widely Used NIR Dye DiR Causes Hypsochromic Shift in Fluorescence Properties. *Eur. J. Pharm. Sci.* **2019**, *132*, 27−33.
(29) Cao, J.; Zhu, B.; Zheng, K.; He, S.; Meng, L.; Song, J.; Yang, H. Recent Progress in NIR-II Contrast Agent for Biological Imaging. *Front. Bioeng. Biotechnol.* **2020**, *7*, No. 487.
(30) Geiser, M.; Kreyling, W. G. Deposition and Biokinetics of Inhaled Nanoparticles. *Part. Fibre Toxicol.* **2010**, *7*, 1−17.
(31) Gustafson, H. H.; Holt-Casper, D.; Grainger, D. W.; Ghandehari, H. Nanoparticle Uptake: The Phagocyte Problem. *Nano Today* **2015**, *10*, 487−510.
(32) Du, B.; Yu, M.; Zheng, J. Transport and Interactions of Nanoparticles in the Kidneys. *Nat. Rev. Mater.* **2018**, *3*, 358−374.
(33) Pardridge, W. M. Drug Transport across the Blood−Brain Barrier. *J. Cereb. Blood Flow Metab.* **2012**, *32*, 1959−1972.
(34) Zhu, M.-T.; Feng, W.-Y.; Wang, Y.; Wang, B.; Wang, M.; Ouyang, H.; Zhao, Y.-L.; Chai, Z.-F. Particokinetics and Extrapulmonary Translocation of Intratracheally Instilled Ferric Oxide Nanoparticles in Rats and the Potential Health Risk Assessment. *Toxicol. Sci.* **2009**, *107*, 342−351.
(35) Henning, A.; Schneider, M.; Nafee, N.; Muijs, L.; Rytting, E.; Wang, X.; Kissel, T.; Grafahrend, D.; Klee, D.; Lehr, C.-M. Influence of Particle Size and Material Properties on Mucociliary Clearance from the Airways. *J. Aerosol Med. Pulm. Drug Delivery* **2010**, *23*, 233−241.
(36) Rao, G. V. S.; Tinkle, S.; Weissman, D.; Antonini, J.; Kashon, M.; Salmen, R.; Battelli, L.; Willard, P.; Hubbs, A.; Hoover, M. Efficacy of a Technique for Exposing the Mouse Lung to Particles Aspirated from the Pharynx. *J. Toxicol. Environ. Health, Part A* **2003**, *66*, 1441−1452.
(37) Patel, B.; Gupta, N.; Ahsan, F. Particle Engineering to Enhance or Lessen Particle Uptake by Alveolar Macrophages and to Influence the Therapeutic Outcome. *Eur. J. Pharm. Biopharm.* **2015**, *89*, 163−174.
(38) Kreyling, W. G.; Hirn, S.; Möller, W.; Schleh, C.; Wenk, A.; Celik, G.; Lipka, J.; Schäffler, M.; Haberl, N.; Johnston, B. D.; Sperling, R.; Schmid, G.; Simon, U.; Parak, W. J.; Semmler-Behnke, M. Air−Blood Barrier Translocation of Tracheally Instilled Gold Nanoparticles Inversely Depends on Particle Size. *ACS Nano* **2014**, *8*, 222−233.
(39) Poon, W.; Zhang, Y.-N.; Ouyang, B.; Kingston, B. R.; Wu, J. L. Y.; Wilhelm, S.; Chan, W. C. W. Elimination Pathways of Nanoparticles. *ACS Nano* **2019**, *13*, 5785−5798.
(40) Mohammad, A. K.; Amayreh, L. K.; Mazzara, J. M.; Reineke, J. J. Rapid Lymph Accumulation of Polystyrene Nanoparticles Following Pulmonary Administration. *Pharm. Res.* **2013**, *30*, 424−434.
(41) Schleh, C.; Semmler-Behnke, M.; Lipka, J.; Wenk, A.; Hirn, S.; Schäffler, M.; Schmid, G.; Simon, U.; Kreyling, W. G. Size and Surface Charge of Gold Nanoparticles Determine Absorption across Intestinal

https://doi.org/10.1021/acs.biomac.2c00221
Biomacromolecules 2022, 23, 2471−2484

Barriers and Accumulation in Secondary Target Organs after Oral Administration. *Nanotoxicology* **2012**, *6*, 36−46.
(42) Hinkley, G. K.; Carpinone, P.; Munson, J. W.; Powers, K. W.; Roberts, S. M. Oral Absorption of PEG-Coated versus Uncoated Gold Nanospheres: Does Agglomeration Matter? *Part. Fibre Toxicol.* **2015**, *12*, No. 9.
(43) Kreyling, W. G.; Holzwarth, U.; Haberl, N.; Kozempel, J.; Wenk, A.; Hirn, S.; Schleh, C.; Schäffler, M.; Lipka, J.; Semmler-Behnke, M.; Gibson, N. Quantitative Biokinetics of Titanium Dioxide Nanoparticles after Intratracheal Instillation in Rats: Part 3. *Nanotoxicology* **2017**, *11*, 454−464.
(44) Schneider, C. S.; Xu, Q.; Boylan, N. J.; Chisholm, J.; Tang, B. C.; Schuster, B. S.; Henning, A.; Ensign, L. M.; Lee, E.; Adstamongkonkul, P.; Simons, B. W.; Wang, S.-Y. S.; Gong, X.; Yu, T.; Boyle, M. P.; Suk, J. S.; Hanes, J. Nanoparticles That Do Not Adhere to Mucus Provide Uniform and Long-Lasting Drug Delivery to Airways Following Inhalation. *Sci. Adv.* **2017**, *3*, No. e160155.
(45) He, X.; Zhang, H.; Ma, Y.; Bai, W.; Zhang, Z.; Lu, K.; Ding, Y.; Zhao, Y.; Chai, Z. Lung Deposition and Extrapulmonary Translocation of Nano-Ceria after Intratracheal Instillation. *Nanotechnology* **2010**, *21*, No. 285103.
(46) Kazemi, A.; Louis, B.; Isabey, D.; Nieman, G. F.; Gatto, L. A.; Satalin, J.; Baker, S.; Grotberg, J. B.; Filoche, M. Surfactant Delivery in Rat Lungs: Comparing 3D Geometrical Simulation Model with Experimental Instillation. *PLOS Comput. Biol.* **2019**, *15*, No. e1007408.
(47) Grotberg, J. B. Respiratory Fluid Mechanics. *Phys. Fluids* **2011**, *23*, No. 021301.
(48) Filoche, M.; Tai, C.-F.; Grotberg, J. B. Three-Dimensional Model of Surfactant Replacement Therapy. *Proc. Natl. Acad. Sci. U.S.A.* **2015**, *112*, 9287−9292.
(49) Leong, B. K. J.; Coombs, J. K.; Sabaitis, C. P.; Rop, D. A.; Aaron, C. S. Quantitative Morphometric Analysis of Pulmonary Deposition of Aerosol Particles Inhaled via Intratracheal Nebulization, Intratracheal Instillation or Nose-Only Inhalation in Rats. *J. Appl. Toxicol.* **1998**, *18*, 149−160.
(50) Kreyling, W. G.; Semmler-Behnke, M.; Takenaka, S.; Möller, W. Differences in the Biokinetics of Inhaled Nano-versus Micrometer-Sized Particles. *Acc. Chem. Res.* **2013**, *46*, 714−722.
(51) Fontana, G.; Licciardi, M.; Mansueto, S.; Schillaci, D.; Giammona, G. Amoxicillin-Loaded Polyethylcyanoacrylate Nanoparticles: Influence of PEG Coating on the Particle Size, Drug Release Rate and Phagocytic Uptake. *Biomaterials* **2001**, *22*, 2857−2865.
(52) Zhong, Q.; Merkel, O. M.; Reineke, J. J.; Da Rocha, S. R. P. Effect of the Route of Administration and PEGylation of Poly(Amidoamine) Dendrimers on Their Systemic and Lung Cellular Biodistribution. *Mol. Pharmaceutics* **2016**, *13*, 1866−1878.
(53) Geiser, M.; Rothen-Rutishauser, B.; Kapp, N.; Schürch, S.; Kreyling, W.; Schulz, H.; Semmler, M.; Hof, V. I.; Heyder, J.; Gehr, P. Ultrafine Particles Cross Cellular Membranes by Nonphagocytic Mechanisms in Lungs and in Cultured Cells. *Environ. Health Perspect.* **2005**, *113*, 1555−1560.
(54) Murata, M.; Tahara, K.; Takeuchi, H. Real-Time in Vivo Imaging of Surface-Modified Liposomes to Evaluate Their Behavior after Pulmonary Administration. *Eur. J. Pharm. Biopharm.* **2014**, *86*, 115−119.
(55) Zhan, X.; Tran, K. K.; Shen, H. Effect of the Poly(Ethylene Glycol) (PEG) Density on the Access and Uptake of Particles by Antigen-Presenting Cells (APCs) after Subcutaneous Administration. *Mol. Pharmaceutics* **2012**, *9*, 3442−3451.
(56) Bustamante-Marin, X. M.; Ostrowski, L. E. Cilia and Mucociliary Clearance. *Cold Spring Harb. Perspect. Biol.* **2017**, *9*, No. a028241.
(57) Nemmar, A.; Hoylaerts, M. F.; Hoet, P. H.; Vermylen, J.; Nemery, B. Size Effect of Intratracheally Instilled Particles on Pulmonary Inflammation and Vascular Thrombosis. *Toxicol. Appl. Pharmacol.* **2003**, *186*, 38−45.
(58) Xiao, J.; Jiang, X.; Zhou, Y.; Sumayyah, G.; Zhou, L.; Tu, B.; Qin, Q.; Qiu, J.; Qin, X.; Zou, Z.; Chen, C. Results of a 30-Day Safety Assessment in Young Mice Orally Exposed to Polystyrene Nanoparticles. *Environ. Pollut.* **2022**, *292*, No. 118184.
(59) Bartneck, M.; Keul, H. A.; Singh, S.; Czaja, K.; Bornemann, J.; Bockstaller, M.; Moeller, M.; Zwadlo-Klarwasser, G.; Groll, J. Rapid Uptake of Gold Nanorods by Primary Human Blood Phagocytes and Immunomodulatory Effects of Surface Chemistry. *ACS Nano* **2010**, *4*, 3073−3086.

https://doi.org/10.1021/acs.biomac.2c00221
Biomacromolecules 2022, 23, 2471−2484